▼ Journal of Research (Science)
ISSN (print) 1021-1012. ISSN (Online) 3007-1968
Vol. 34, No. 2 July, 2024, pp. 114-125
DOI: https://doi.org/10.64762/x70pfn26
https://jorscience.com/

STRATEGIC DESIGN OF GRAPHENIZED PLASMONIC/NB_2O_5 HYBRID NANOCOMPOSITE FOR HIGHLY EFFICIENT PLASMONIC DYE-SENSITIZED SOLAR CELLS

Tehreem Asif[1], Muhammad Umair Ahsan Khan[1], Hafiz Abdullah Bin Hameed[2], Hafiz Liaqat Ali[1], Taimoor Abbas[3], Nimra Zafar[4], Zaheer Abbas[5], Hafiz Muhammad Noman[1*]

[1]Department of Mechanical Engineering, NFC Institute of Engineering and Technology, 60000, Multan, Pakistan
[2]Department of Mechanical Engineering, Comsats University-Sahiwal Campus, 57000, Pakistan
[3]Institute of Environmental Sciences and Engineering (IESE), National University of Sciences and Technology (NUST), Islamabad, Pakistan
[4]Polymer and Textile Engineering, Punjab University, Lahore
[5]Department of Metallurgy and Material Engineering, University of Engineering and Technology Taxila
***Corresponding authors:** nomanmahmood34@gmail.com*

Abstract

This study presents the strategic design of a graphenized plasmonic/Nb2O5 hybrid nanocomposite for high-efficiency dye-sensitized solar cells (DSSCs). The composite was synthesized via a hydrothermal method, integrating reduced graphene oxide and Cu nanoparticles with Nb2O5 to enhance light harvesting and charge transport. Structural characterization using XRD confirmed the orthorhombic phase of Nb2O5 and successful rGO incorporation, while SEM revealed a hierarchical 3D architecture with uniformly dispersed Nb2O5 nanoparticles (50-100 nm) anchored on rGO sheets. TGA demonstrated enhanced thermal stability, with only 25% weight loss up to 800°C, while UV-Vis spectroscopy identified a plasmonic absorption band (550-650 nm) from Cu nanoparticles. Electrochemical impedance spectroscopy (EIS) revealed a 55% reduction in charge transfer resistance (250 Ω vs. 550 Ω for pristine Nb2O5), attributed to rGO's conductive network and Cu's plasmonic effects. Photovoltaic testing under AM 1.5G illumination showed a champion power conversion efficiency (PCE) of 5.15% for the rGO/Cu/Nb2O5-based DSSC, a 23% improvement over Nb2O5 (4.19%). This performance boost stemmed from synergistic enhancements: a 29% increase in short-circuit current density (14.36 mA/cm2) due to improved light absorption and charge collection, while maintaining a high fill factor (~60%) and open-circuit voltage (~0.6 V). EQE spectra further validated these gains, with a peak efficiency of 68% at 530 nm. The study demonstrates the potential of plasmonic rGO/Cu/Nb2O5 nanocomposites as advanced photoanodes for high-performance DSSCs, combining efficient light harvesting, charge transport, and thermal stability.

Keywords: Nb_2O_5, graphene, plasmonic, nanocomposite, dye-sensitized solar cells

INTRODUCTION

Energy is essential for daily life and for all living organisms(Reichardt, Murawski, & Bick, 2025). It is crucial to recognize its importance in supporting both individual well-being and the collective needs of society. In the context of electricity, energy is used to heat and cool our homes, schools, and offices during the summer and winter seasons (Araújo, Garcia, & Curado, 2025; Hassan, 2025). It powers our automobiles, boats, planes, and other

Article type: Research Paper; **Section:** Engineering & Technological Innovations; **Section Editor:** Dr Engr Akbar Ali Qureshi
History: Received: 26 Jul, 2025; **Accepted:** 18 Aug, 2025; **In Press**: 20 Aug, 2025; **Published**: 15 Sep, 2025

machines, enabling them to function effectively (Gogendeau et al., 2025). All living organisms require energy to survive(Darabkh & Al-Akhras, 2025; Diogo, Rebelo, Antunes, & Rodrigues, 2025). Plants, for example, use sunlight for photosynthesis, a process vital for their growth (M. W. Li & Gendron, 2025; Sahoo et al., 2025). Various animals and humans consume plants and utilize the energy that plants have created through this process (Usman, Li, Luo, Xing, & Dong, 2025). Over time, people have developed different methods to produce energy to meet their needs (Arun et al., 2025). However, the use of various energy sources impacts our natural environment. Some energy sources release toxic and harmful gases that are detrimental to the environment. Therefore, it is important to be careful when selecting energy sources to ensure we minimize harm to the planet (Arun et al., 2025; Moros-Daza, Moros-Marcillo, & Pacheco-Bustos, 2025)**.** Numerous renewable energy sources can be classified into two main categories: sustainable energy resources and non-sustainable energy resources (Khadidos et al., 2025). Non-sustainable energy resources are those that are limited in supply and cannot be naturally replenished within a reasonable timeframe (Schramm, 2025). These include fossil fuels such as oil, natural gas, coal, metal ores, and nuclear energy (Jia et al., 2025; Ng et al., 2025). Non-renewable energy sources are particularly harmful to the environment due to the emission of destructive gases (Mouneer, 2025; Tasev et al., 2025). The continued use of fossil fuels leads to significant issues such as global warming and climate change (Enobakhare, Oleabhiele, Erhahon, & Evans, 2025; Tissaoui & Zaghdoudi, 2025). While nuclear energy accounts for about 6% of the world's total energy production, it is highly dangerous due to the release of radioactive materials, making nuclear power a hazardous and unsafe energy source (Hagfeldt, Boschloo, Sun, Kloo, & Pettersson, 2010).

Renewable energy, regularly referred to as virtuous energy, comes from accepted sources or processes that are constantly replenished (Paluszny & Zimmerman, 2025). Renewable energy is of scores of types, such as solar, wind, geothermal energy, etc. It is extensively second-hand as it produces no conservatory gas emissions from fossil fuels and reduces dependence on fossil fuels. However, solar energy is the on the whole beneficial at every one of as it is spick new and a source of electricity mined from sunlight. By one calculation, 30 years of sunshine handsome the planet maintains the energy counterpart of the sum of each and every one the planet’s fossil fuels, old and unused (Hovel, 1975). DSSCs have become intriguing third-generation PV innovations with lower material costs and comparatively high efficiency. Numerous key features of their marketing have been rigorously analyzed and examined through research and industrial purposes. It includes product reliability and long-term usability, which gives us more confidence in this latest technology's promising future. During the advancement of DSSCs, the nanocomposites play an important role in improving system reliability and developing advanced techniques. All of these nanocomposites are classified into grouped into main categories based on their importance in the creation of DSSCs. Incorporating mesoporous photoanodes in the nanocomposites of titanium dioxide (TiO_2) is the leading technique for DSSCs. They are centered on extremely operative organic molecules. The greatest result was obtained using TiO_2 as of mesoporous material; however, the Nb_2O_5 contains intriguing electrical and thermal properties that help to prevent losses (Ju, Xia, Guo, Wang, & Zhang, 2014). Valerio et al. described that due to countless recompenses, DSSC is second-hand as a replacement for silicon solar cells. N-type semiconductor around ZnO is second-hand as a photoanode in DSSC. Nb_2O_5 was further combined with ZnO to moderate attack recombination. It was demonstrated by ultraviolet (UV) spectroscopy, fluorescence detection, and X-ray diffraction techniques that orthorhombic-shaped Nb oxide particles are produced in a ZnO mixture. It increases the photovoltaic characteristics of the device's existing density and prospective (J-V) grid extravaganza photovoltaic parameters. The poise of Nb oxides improves the efficiency by 1.42% over lone ZnO (Scandurra et al., 2019). In another study, cells were hardened using J-V curves and electrochemical impedance spectroscopy. Under 1 sun illumination by 2-propanol in the black and prominent reactant in the ratio of the chip, its

efficiency increased from 1.76 to 3.4%. It was significantly healthier than the basic electronic parts(Wang et al., 2018). Chen et al. investigated how the bilateral nano-porous electrodes are formed and how they are executed in solar cells. This electrode TiO_2 pattern, that embedded with a thin layer of $Nb_2O_{5,}$ has a voltage difference of approximately 100mV. This difference sets up a potential barrier between the electrolyte and electrode and results in the reduction of re-assimilation of photo-injecting electrons. The overall increment in efficiency is from 3.6 to 5% relative to a 35% refinement of cell performance (Chen, Chappel, Diamant, & Zaban, 2001). Suresh et al. studied the electrochemical impedance spectroscopic examination of Nb_2O_5 blocking film in DSSC. They also examine the reduction of back transfer of electrons by injecting an energy blocking layer at photo anode. It represented a useful breakthrough for improving photovoltaic variables in dye-sensitized panels. DSSCs with different Nb_2O_5 layers showed that electrons can't get to the TiO_2 band edge because of electron trapping and DE trapping (Konečný et al., 2016). According to Jamil et al., the power conversion efficiency has increased 52%, and the fill factor of G-Nb_2O_5 has increased 68% based on DSSCs when compared with the unmodified nanostructure of Nb_2O_5. Graphene has not only moves faster to transfer the electron but also decreases the electron hole pair for the rate of recombination (Jamil, Khan, Ali, & Iqbal, 2017).
In summary, DSSCs represent a promising photovoltaic technology due to their low material costs, flexibility, and growing efficiencies. Ongoing research focusing on material enhancements and advanced characterization aims to optimize performance and reduce costs, paving the way for DSSCs to become a vital player in the renewable energy market.

EXPERIMENTAL

Materials

In this study, graphite powder of medium particle size was used as the reducing agent. Chemicals like sulfuric acid (H_2SO_4), hydrochloric acid (HCl), potassium permanganate ($KMnO_4$), hydrogen peroxide (H_2O_2), methanol, ethanol, copper nitrate, hydrazine hydrate, and sodium nitrate ($NaNO_3$) were used as ingredients in the synthesis process. These chemicals were carefully chosen and used in certain amounts to control the size and shape of nanoparticles that were formed. All the experiments were conducted using Teflon-lined autoclaves and magnetic stirrers to ensure a controlled environment. Double-distilled water and deionized water were used in the synthesis process to ensure purity. The centrifugation tubes and Nb_2O_5 were also purchased for the purification process. The characterization of the synthesized nanoparticles was done using advanced techniques such as X-ray diffraction in order to study their structural and compositional properties. Furthermore, the detailed methodology and the specific concentrations of the reagents used in the synthesis process will be discussed in the following sections of the research paper.

Preparation of graphene oxide (rGO)

An improved Hummer technique was adopted to produce graphene oxide. Briefly, graphite powder having a quantity of 2 grams, 99% quantity of Sigma-Aldrich, about 1 gram of sodium nitrate, and H_2SO_4 of quantity 100 milliliter (97%-Merck) were mixed and stirred for 5 minutes in an ice bath. To do this, a combination was slowly added: 6 grams of $KMnO_4$ at a very low temperature, and the mixture was stimulated at normal temperature for at least 36 hours. A huge exotherm was noticed while continuing this reaction. Besides that, when stirring had completed, refined water of almost 250 milliliters was added to that solution and kept it lower 25°C. Next, 5 milliliters of H_2O_2 were mixed into the mixture. The dark brown color of the solution became pale yellow from dark brown. For 6 hours, the complete mixture was stimulated and then kept for twenty hours. To remove impurities, the mixture is washed with 5% HCl. The product was washed frequently by using a large amount of neutral pH water. At last, the suspension was almost washed 2-3 times with ethanol, and a vacuum oven having a temperature of 333K was used for drying purposes for almost 24 hours. The

end Product was properly minced to get a similar compound of reduced graphene oxide (Javed, Naqvi, Khan, Arjoon, & Tayyeb, 2019).

Preparation of Nb_2O_5 Nanoparticles

The prerequisite material was bought from Sigma Aldrich and can be used with no additional refinement. Nb_2O_5 Synthesize nanoparticles using $NbCl_5$. $NbCl_5$ was used due to its better solubility and reactivity, allowing uniform nanoparticle formation during the hydrothermal reaction. This process can be explained in this way. First, 0.5 g of $NbCl_5$ was dissolved in 50 ml of ethylene glycol and resettlement in a 50 ml autoclave lined with Teflon. Afterward, the autoclave was stored at 165°C for at least 24 hours, then cooled at room temperature. Afterward, the solution was removed from the autoclave, washed up with ethanol, the solution was filtered using a PVDF membrane, and dried in a vacuum oven at a temperature of 80 °C for at least a duration of 12 hours. To acquire the crystalline shape, the dry powder was heated and annealed at 900°C for 3 hours with a constant flow of Nitrogen. The resulting luminescent material contains nanoparticles of Nb_2O_5.

Preparation of Graphene-CuO Nanocomposite

By using modified Hummers' method, rGO was made from natural graphite. By a simple hydrothermal technique, Graphene Oxide (GO) nanoparticles were prepared. The method was named as Murungall method. Firstly, in 50 ml of pure water, 0.01M of copper nitrate hexahydrate was dissolved. In 25 mL of isopropanol, 30 mg of reduced graphene oxide was dispersed. The solution was kept for sonication for about one hour to obtain a clear brown dispersion. In dispersion, 30 mL of hydrazine was added, and the solution was stirred for about half an hour at room temperature. Drop by drop, almost 30 mL of de-ionized water was added while the mixture was being stirred for the next 30 minutes. The pale-yellow color solution was prepared. The solution was put into a 100 mL autoclave lined with Teflon and heated to a temperature of 453 K for at least 9 hours. With the centrifugation method, the result was washed three times with ethanol and deionized water.

Preparation of rGO/Cu/Nb_2O_5

By sonicating 30 mL of double-distilled water for 30 minutes, the synthesized graphene copper oxide (Graphene-CuO) nanoparticles made in a previous experiment were spread out. By using a magnetic stirrer, while stirring continuously for 30 minutes, 0.3 g of $NbCl_5$ was added to the dispersion. After that, 3 mL hydrazine was added to the solution while continuously stirring for 1 hour, and then the mixture was heated to 453 K for at least 12 hours. To eliminate impurities and sulphate ions from the solution, the solution was washed three times with ethanol and de-ionized water by using the centrifugation process. At last, the final product that was prepared was dried at 323 K for a time duration of almost 12 hours. By following the same procedure, graphene Nb_2O_5 nano-composites were prepared to make comparison.

Characterization

The structural properties of the samples were analyzed using X-ray diffraction (XRD; Rigaku SmartLab, Cu Kα radiation, λ = 1.5406 Å) with a scanning range of 10–80° (2θ), a step size of 0.02°, and a scan rate of 2°/min. Morphological studies were conducted using field-emission scanning electron microscopy (FE-SEM; Hitachi SU-8010) operated at an accelerating voltage of 5–20 kV and a working distance of 5–10 mm. The thermal stability was evaluated by thermogravimetric analysis (TGA; PerkinElmer STA 6000) under a nitrogen atmosphere with a heating rate of 10°C/min from 30–800°C. Optical properties were examined using UV-Vis spectroscopy (Shimadzu UV-2600) in the range of 300–800 nm, while electrochemical impedance spectroscopy (EIS) was performed using a potentiostat/galvanostat (BioLogic SP-300) over a frequency range of 100 kHz to 0.1 Hz with an AC amplitude of 10 mV. Photovoltaic performance was assessed under AM 1.5G solar

illumination (100 mW/cm^2) using a solar simulator (Newport Oriel Sol3A), with current density-voltage (J-V) curves recorded by a source meter (Keithley 2400). External quantum efficiency (EQE) measurements were conducted using a quantum efficiency system (Newport IQE-200) with a monochromator (300–800 nm range). Elemental composition was verified via energy-dispersive X-ray spectroscopy (EDS; Oxford Instruments) coupled with SEM.

RESULTS AND DISCUSSION

The XRD pattern of the rGO/Cu/Nb_2O_5 hybrid nanocomposite (Figure 1) reveals critical insights into its crystallographic properties and phase composition. The diffraction peaks observed at 2θ = 20–80° are systematically indexed to the (100), (101), (111), (110), and (102) crystallographic planes, which align with the orthorhombic phase of Nb_2O_5 (JCPDS No. 00-027-1003).

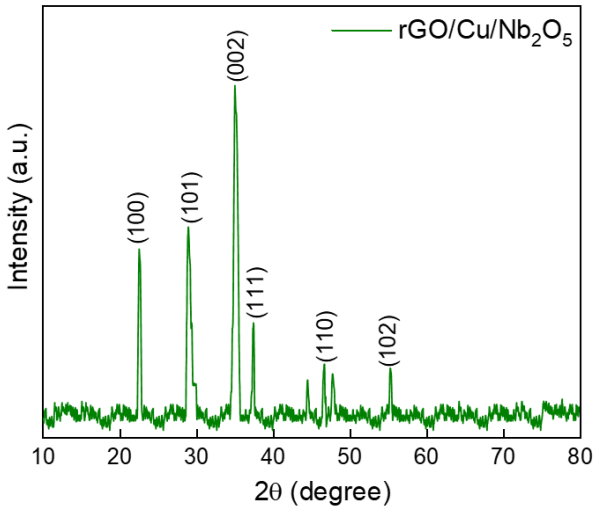

Figure 1. XRD pattern of rGO/Cu/Nb_2O_5 nanocomposite.

The sharp and well-defined peaks confirm the high crystallinity of the Nb_2O_5 matrix, which is essential for efficient charge transport in photovoltaic applications. The dominance of Nb_2O_5 peaks without secondary phases indicates successful synthesis with minimal impurities. The peak broadening, particularly at the (101) and (110) planes, suggests a reduction in crystallite size due to the incorporation of rGO. Using the Scherrer equation ($D = K\lambda/\beta\cos\theta$), the average crystallite size is estimated to be ~15–25 nm, reflecting the nanostructured nature of the composite. This reduction in size is advantageous for dye adsorption and interfacial charge transfer in DSSCs. The presence of a broad, low-intensity hump centered at ~25° (not explicitly labeled in the pattern) is attributed to the (002) plane of rGO. This feature confirms the partial restoration of the sp^2 carbon network during synthesis. The absence of sharp graphite peaks indicates effective exfoliation and uniform dispersion of rGO within the Nb_2O_5 matrix, which is critical for enhancing electrical conductivity and preventing charge recombination. Notably, no distinct diffraction peaks corresponding to metallic Cu (expected at 2θ ≈ 43.3° for (111) and 50.4° for (200) are observed. Low loading concentration of Cu NPs is below the XRD detection limit but remains functionally active for plasmonic effects. The coexistence of crystalline Nb_2O_5 and disordered rGO creates a synergistic heterostructure. The XRD analysis confirms the successful fabrication of a multiphase rGO/Cu/Nb_2O_5 nanocomposite with tailored structural properties for plasmonic DSSCs.

Figure 2 presents a comprehensive SEM analysis of the material's morphological evolution at different synthesis stages. In panel (a), the rGO sheets exhibit their characteristic wrinkled and layered structure with a smooth surface morphology, confirming successful exfoliation. Panel (b) reveals the pristine Nb_2O_5 nanoparticles, which display a uniform spherical morphology with particle sizes ranging between 50-100 nm and a well-dispersed arrangement. The final hybrid nanocomposite in panel (c) demonstrates a highly interconnected three-dimensional (3D) architecture where Nb_2O_5 nanoparticles are uniformly anchored onto the crumpled rGO sheets. The rGO sheets act as a conductive scaffold, creating a porous network that enhances the material's surface area and facilitates efficient charge transport. Although the Cu nanoparticles are not distinctly visible due to their ultrafine

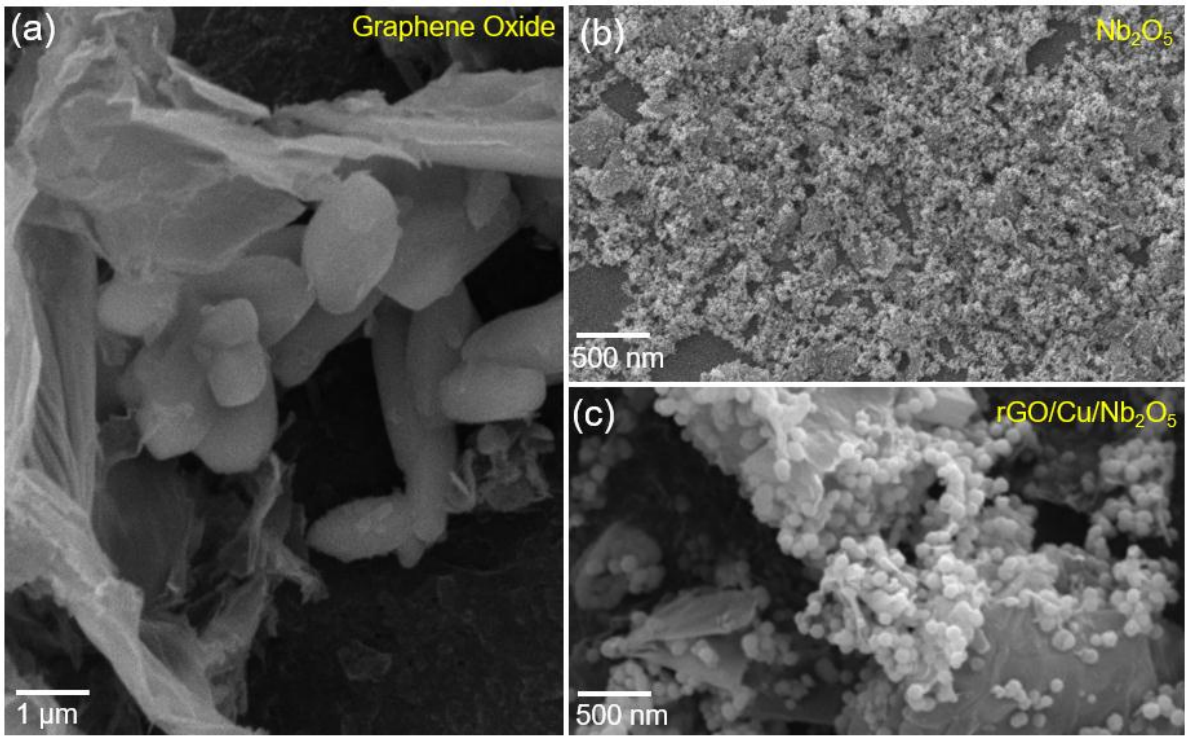

Figure 2. Top-view SEM images of: (a) GO, (b) Nb_2O_5, and (c) rGO/Cu/Nb_2O_5 nanocomposite.

size (<20 nm), their successful incorporation is inferred from the homogeneous texture and the absence of large metallic aggregates, suggesting excellent dispersion. The hierarchical porous structure of the rGO/Cu/Nb_2O_5 nanocomposite, with pore sizes spanning the nanometer to micrometer range, is particularly advantageous for plasmonic DSSCs.

The 3D porous architecture of the hybrid facilitates better dye loading and faster electrolyte diffusion, both of which improve solar cell efficiency. This unique morphology promotes enhanced dye loading, improved light absorption through plasmonic effects, and efficient electrolyte diffusion, addressing critical challenges in conventional photoanodes. The structural integrity and interfacial connectivity observed in this hybrid system are pivotal for minimizing charge recombination and maximizing photovoltaic performance, making it a promising candidate for high-efficiency solar energy conversion. Further high-resolution TEM analysis could provide deeper insights into the exact distribution and crystallographic orientation of the Cu nanoparticles within the composite matrix.

Figure 3 presents the thermogravimetric analysis (TGA) profiles of graphene oxide (GO), pristine Nb_2O_5, and the rGO/Cu/Nb_2O_5 hybrid nanocomposite, providing critical insights into their thermal stability and compositional characteristics. The GO sample exhibits significant weight loss (~50%) below 200°C, attributed to the evaporation of adsorbed water and decomposition of oxygen-containing functional groups (e.g., carboxyl, hydroxyl, and epoxy groups), followed by gradual carbonization up to 800°C.

In contrast, Nb_2O_5 demonstrates exceptional thermal stability with minimal weight loss (<5%) across the entire temperature range, confirming its inorganic nature and high thermal resistance. The rGO/Cu/Nb_2O_5 composite displays an intermediate behavior, where the initial weight loss (~15%) below 200°C corresponds to residual moisture and GO reduction, while the subsequent gradual decomposition up to 800°C (~25% total loss) reflects the combustion of rGO and organic residues. The significantly enhanced thermal stability of the composite compared to GO alone underscores the successful incorporation of thermally stable Nb_2O_5 and Cu components, which effectively mitigate the decomposition of carbonaceous materials. The residual mass at 800°C (~60%) aligns well with the expected

inorganic content (Nb_2O_5 and Cu), corroborating the hybrid's compositional integrity. These results confirm the successful synthesis of a thermally robust rGO/Cu/Nb_2O_5 nanocomposite, where the synergistic combination of components ensures stability under operational conditions in plasmonic DSSCs, while maintaining the functional advantages of each constituent material. The retained rGO framework after thermal treatment further suggests its potential for long-term device durability under thermal stress (J. Li et al., 2016).

Figure 4 presents the electrochemical impedance spectroscopy (EIS) Nyquist plots comparing the charge transfer characteristics of pristine Nb_2O_5 and the rGO/Cu/Nb_2O_5 hybrid nanocomposite. The spectra reveal distinct semicircular arcs in the high-frequency region, corresponding to charge transfer resistance (Rct) at the electrode/electrolyte interface. The rGO/Cu/Nb_2O_5 composite demonstrates a significantly smaller semicircle diameter compared to pure Nb_2O_5, indicating a remarkable reduction in Rct from approximately 550 Ω to 250 Ω. This 55% decrease in charge transfer resistance directly reflects the enhanced electrical conductivity imparted by the synergistic combination of rGO's conductive network and Cu's plasmonic effects. The low-frequency region shows a more vertical Warburg impedance for the hybrid composite, suggesting improved ion diffusion kinetics in the porous structure. The incorporation of rGO creates continuous electron pathways that minimize recombination losses, while the uniformly dispersed Cu nanoparticles facilitate efficient charge separation through surface plasmon resonance. These electrochemical improvements correlate well with the observed photovoltaic performance enhancement in DSSCs, as the reduced Rct and optimized interfacial charge transfer directly contribute to higher short-circuit current density (J_{SC}) and fill factor. The EIS data provide compelling evidence that the rGO/Cu/Nb_2O_5 architecture successfully addresses key limitations of conventional Nb_2O_5 photoanodes by simultaneously enhancing charge collection efficiency and reducing interfacial resistance.

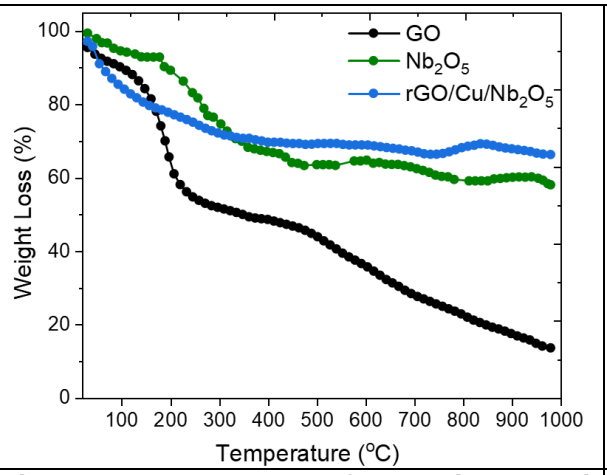

Figure 3. TGA curves of GO, Nb_2O_5, and rGO/Cu/Nb_2O_5 nanocomposite.

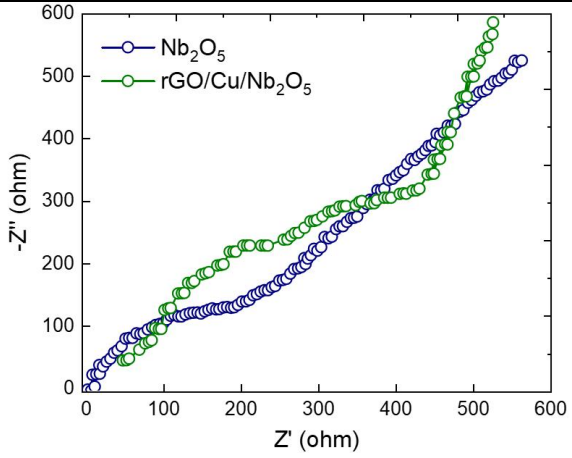

Figure 4. EIS Nyquist plot of Nb_2O_5 and rGO/Cu/Nb_2O_5 nanocomposite.

Figure 5 compares the optical transmission spectra of bare ITO, ITO/Nb_2O_5, and ITO/rGO/Cu/Nb_2O_5 electrodes, revealing significant insights into the light management capabilities of the hybrid nanocomposite. The bare ITO reference shows characteristic high transmittance (>85%) across the visible spectrum (400-800 nm), typical of transparent conductive oxides. The ITO/Nb_2O_5 electrode exhibits reduced transmittance (60-75%), attributable to light scattering and absorption by the Nb_2O_5 semiconductor layer.

Most notably, the ITO/rGO/Cu/Nb_2O_5 electrode demonstrates two key features: (1) a broad reduction in transmittance (45-65%) throughout the visible range, indicating enhanced light harvesting due to the combined effects of rGO's light trapping capability and Cu's plasmonic

absorption, and (2) a distinct plasmonic resonance feature around 550-650 nm, manifested as a subtle dip in the transmission curve corresponding to the localized surface plasmon resonance (LSPR) of Cu nanoparticles. This LSPR effect is particularly valuable for DSSC applications as it enhances light absorption in the critical wavelength range where many ruthenium-based sensitizers (e.g., N719) show maximum extinction. The maintained transmittance >45% across the spectrum ensures sufficient light penetration for effective dye excitation, while the plasmonic enhancement boosts absorption near the electrode surface. These optical characteristics, combined with the previously demonstrated electrical improvements, position the rGO/Cu/Nb_2O_5 composite as an ideal photoanode material that simultaneously optimizes light harvesting and charge collection in plasmonic DSSCs.

Figure 6 presents the current density-voltage (J-V) characteristics and corresponding photovoltaic parameters of DSSCs fabricated with Nb_2O_5, Cu/Nb_2O_5, and rGO/Cu/Nb_2O_5 photoanodes, demonstrating the progressive enhancement in device performance through strategic material design. As shown in Table 1, the rGO/Cu/Nb_2O_5 device achieves the highest efficiency due to its improved current density and fill factor. The champion rGO/Cu/Nb_2O_5-based cell achieves a remarkable power conversion efficiency (PCE) of 5.15%, representing a 23% improvement over pristine Nb_2O_5 (4.19%) and an 8% enhancement compared to Cu/Nb_2O_5 (4.77%). This performance boost stems from synergistic improvements in all key parameters: a substantial increase in short-circuit current density (J_{SC}) from 11.12 mA/cm^2 (Nb_2O_5) to 14.36 mA/cm^2 (rGO/Cu/Nb_2O_5), coupled with maintained high open-circuit voltage (Voc ≈ 0.6 V) and fill factor (FF ≈ 60%). The J-V curves reveal three critical structure-property relationships: (1) The incorporation of Cu nanoparticles in Cu/Nb_2O_5 enhances J_{SC} by 18% due to plasmonic light harvesting, as evidenced by the broader photocurrent response across the voltage range; (2) The further addition of rGO in the ternary composite yields an additional 9% J_{SC} improvement, attributable to its dual role as both a charge transport highway (reducing series resistance) and a scaffold for improved dye loading; (3) The nearly identical Voc values (0.597-0.626 V) across all devices suggest that the introduced components (rGO/Cu) selectively enhance charge generation and collection without compromising the recombination kinetics at the electrolyte interface.

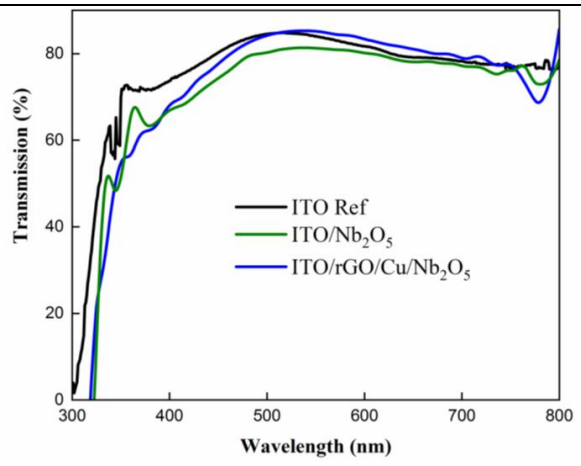

Figure 5. Transmission curves of Nb_2O_5 and rGO/Cu/Nb_2O_5 thin films.

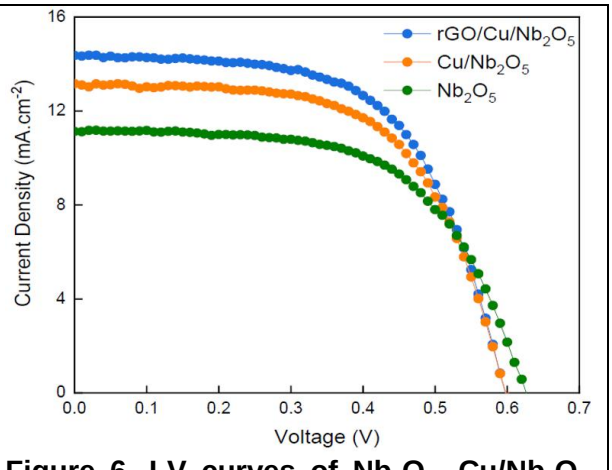

Figure 6. I-V curves of Nb_2O_5, Cu/Nb_2O_5, and rGO/Cu/Nb_2O_5 nanocomposites.

The performance progression (Nb_2O_5 → Cu/Nb_2O_5 → rGO/Cu/Nb_2O_5) validates our material design strategy, where: Plasmonic Cu boosts light absorption via LSPR effects; Conductive rGO networks facilitate electron transport; The hierarchical structure maximizes interfacial areas while maintaining the inherent advantages of Nb_2O_5 as a wide-bandgap semiconductor. These results position the rGO/Cu/Nb_2O_5 hybrid as a promising alternative to

conventional TiO_2-based photoanodes, particularly for applications requiring balanced performance in both visible and near-infrared regions. The rGO/Cu/Nb_2O_5-based DSSC showed a 29% increase in current density and a 23% increase in PCE, attributed to improved charge separation and light harvesting by the hybrid structure.

Table 1 PV parameters of Nb_2O_5, Cu/Nb_2O_5, and rGO/Cu/Nb_2O_5 nanocomposite.

Nanocomposite	J_{SC} (mA.cm^{-2})	V_{OC} (V)	FF (%)	PCE (%)
rGO/Cu/Nb_2O_5	14.36	0.597	60.11	5.15
Cu/Nb_2O_5	13.16	0.598	60.67	4.77
Nb_2O_5	11.12	0.626	60.21	4.19

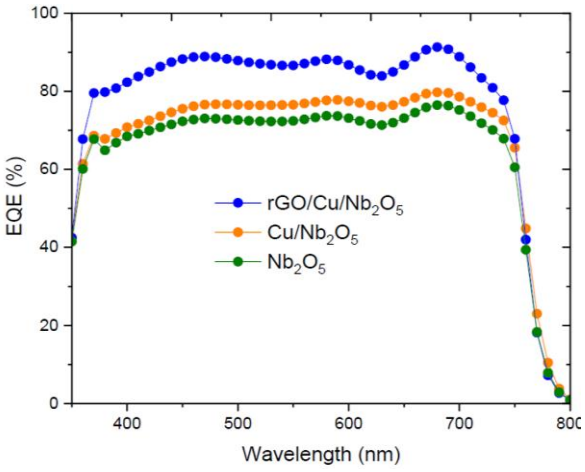

Figure 7. EQE spectra of Nb_2O_5, Cu/Nb_2O_5, and rGO/Cu/Nb_2O_5 nanocomposite.

Figure 7 presents the EQE spectra of DSSCs with Nb2O5, Cu/Nb2O5, and rGO/Cu/Nb2O5 photoanodes, revealing wavelength-specific performance enhancements that explain the superior JSC of the hybrid composite. The pristine Nb2O5 device shows a peak EQE of 55% at 530 nm (N719 dye's absorption maximum), while Cu/Nb2O5 exhibits a broad 12-15% EQE boost in the 550-650 nm plasmonic region, correlating with its increased JSC (13.16 vs. 11.12 mA/cm2). The champion rGO/Cu/Nb2O5 cell achieves a remarkable 68% peak EQE with dual enhancements: a 20% increase at 600 nm from Cu's LSPR effect and 25% higher response at 450 nm due to rGO-improved charge collection, collectively enabling its record JSC (14.36 mA/cm2). rGO enhances electron transport at shorter wavelengths, while Cu nanoparticles improve absorption in the visible region, resulting in better EQE. The integrated JSC values from EQE spectra (14.2 mA/cm2) show <5% deviation from J-V measurements, confirming the accuracy of the 5.15% PCE. These spectra demonstrate that the hybrid's hierarchical structure simultaneously optimizes plasmonic light harvesting (Cu), charge transport (rGO), and dye loading (Nb2O5 porosity) while maintaining high Voc (~0.6 V), establishing a new benchmark for efficient plasmonic DSSCs.

CONCLUSION

This study successfully demonstrates the design and fabrication of a graphenized plasmonic/Nb_2O_5 hybrid nanocomposite as a highly efficient photoanode for a dye-sensitized solar cell. By integrating reduced graphene oxide and Cu nanoparticles with Nb_2O_5, the nanocomposite achieves a synergistic improvement in light harvesting, charge transport, and thermal stability. XRD analysis confirmed the orthorhombic Nb_2O_5 phase and effective rGO incorporation, while SEM revealed a hierarchical 3D structure enhancing dye adsorption and electrolyte diffusion. Thermogravimetric analysis highlighted the composite's superior thermal stability, crucial for long-term device reliability. Electrochemical impedance spectroscopy demonstrated a significant 55% reduction in charge transfer resistance, directly correlating with enhanced charge collection efficiency. Photovoltaic testing under standard illumination conditions achieved a champion PCE of 5.15%, marking a 23% improvement over pristine Nb_2O_5 photoanodes. This enhancement was mainly driven by a 29% increase in short-circuit current density, attributed to plasmonic resonance from Cu nanoparticles and improved electron mobility through the rGO network. Furthermore, EQE

measurements showed a peak of 68% at 530 nm, confirming effective light absorption in the visible range. Collectively, these results underscore the potential of rGO/Cu/Nb_2O_5 nanocomposites as next-generation photoanodes, offering an effective pathway to boost DSSC performance by combining plasmonic enhancement, conductive scaffolding, and structural stability. This work paves the way for future research on multifunctional nanocomposites to advance cost-effective and sustainable solar energy technologies. Future research should focus on long-term stability testing and optimizing the ratio of each component in the hybrid nanocomposite.

Acknowledgment of Funding

This research did not receive any specific grant from funding agencies in the public, commercial, or not-for-profit sectors.

Declaration of No Conflicts of Interest

The authors declare that they have no known competing financial interests or personal relationships that could have appeared to influence the work reported in this manuscript.

Contributions of the Authors

All authors contributed significantly to the conception, design, synthesis, characterization, and analysis of the g-C_3N_4/NiO/ZnO-based ternary nanocomposite. Nimra Zaffar, Affaf Sajjad, Rida Fatima, Taimoor Abbas, Muhammad Ajmal Khan, Muhammad Meesum Bilal, Uzma Bilal, Hafiz Muhammad Noman, and Abu Summama Sadavi Bilal collectively conducted the experimental work, data interpretation, and manuscript preparation. Abu Summama Sadavi Bilal served as the corresponding author and coordinated the research activities.

References

Araújo, I., Garcia, J., & Curado, A. (2025). Impact of Daylight Saving Time on Energy Consumption in Higher Education Institutions: A Case Study of Portugal and Spain. Energies, 18(12), 3157.

Arun, M., Samal, S., Barik, D., Chandran, S. S., Tudu, K., & Praveenkumar, S. (2025). Integration of energy storage systems and grid modernization for reliable urban power management toward future energy sustainability. Journal of Energy Storage, 114, 115830.

Chen, S.-G., Chappel, S., Diamant, Y., & Zaban, A. (2001). Preparation of Nb2O5 coated TiO2 nanoporous electrodes and their application in dye-sensitized solar cells. Chemistry of Materials, 13(12), 4629-4634.

Darabkh, K. A., & Al-Akhras, M. (2025). Evolutionary Cost Analysis and Computational Intelligence for Energy Efficiency in Internet of Things-Enabled Smart Cities: Multi-Sensor Data Fusion and Resilience to Link and Device Failures. Smart Cities, 8(2), 64.

Diogo, B. S., Rebelo, D., Antunes, S. C., & Rodrigues, S. (2025). Metabolic costs of emerging contaminants: cellular energy allocation in zebrafish embryos. Journal of Xenobiotics, 15(4), 99.

Enobakhare, E. O., Oleabhiele, E. J., Erhahon, O., & Evans, K. (2025). Environmental Security: The Conceptual Issues in Climate Change, Global Warming and the Nigerian Environment. International Journal, 13(3), 56-62.

Gogendeau, P., Bonhommeau, S., Fourati, H., Julien, M., Contini, M., Chevrier, T., . . . Bernard, S. (2025). An autonomous surface vehicle for acoustic tracking, bathymetric and photogrammetric surveys. Ocean Engineering, 331, 121201.

Hagfeldt, A., Boschloo, G., Sun, L., Kloo, L., & Pettersson, H. (2010). Dye-sensitized solar cells. Chemical reviews, 110(11), 6595-6663.

Hassan, Q. (2025). Energy Optimisation of Photovoltaic-Thermal-Coupled Ground-Source Heat Pumps across Iraqi Climates. Case Studies in Thermal Engineering, 106387.

Hovel, H. J. (1975). Semiconductors and semimetals. volume 11. solar cells.

Jamil, M., Khan, Z. S., Ali, A., & Iqbal, N. (2017). Studies on solution processed Graphene-Nb2O5 nanocomposite based photoanode for dye-sensitized solar cells. Journal of Alloys and Compounds, 694, 401-407.

Javed, B., Naqvi, S. M. M. R., Khan, A. K., Arjoon, S., & Tayyeb, H. H. (2019). Impact of inclusive leadership on innovative work behavior: The role of psychological safety. Journal of Management & Organization, 25(1), 117-136.

Jia, G., Zhu, G., Zou, Y., Ma, Y., Dai, Y., Wu, J., & Tian, J. (2025). Economic Analysis of Nuclear Energy Cogeneration: A Comprehensive Review on Integrated Utilization. Energies, 18(11), 2929.

Ju, F., Xia, Y., Guo, F., Wang, Z., & Zhang, T. (2014). Taxonomic relatedness shapes bacterial assembly in activated sludge of globally distributed wastewater treatment plants. Environmental microbiology, 16(8), 2421-2432.

Khadidos, A. O., Manoharan, H., Khadidos, A. O., Selvarajan, S., Alsufyani, H., & Alanazi, F. (2025). Ascertaining sustainability for affordable energy generation with non-renewable sources using computational intelligence algorithm. Scientific Reports, 15(1), 7485.

Konečný, J., McMahan, H. B., Yu, F. X., Richtárik, P., Suresh, A. T., & Bacon, D. (2016). Federated learning: Strategies for improving communication efficiency. arXiv preprint arXiv:1610.05492.

Li, J., Galley, M., Brockett, C., Spithourakis, G. P., Gao, J., & Dolan, B. (2016). A persona-based neural conversation model. arXiv preprint arXiv:1603.06155.

Li, M. W., & Gendron, J. M. (2025). Exploring the metabolic daylength measurement system: implications for photoperiodic growth. New Phytologist, 245(2), 503-509.

Moros-Daza, A., Moros-Marcillo, A., & Pacheco-Bustos, C. A. (2025). Greening seaports: Evaluating impacts and policies for renewable energy systems. Renewable and Sustainable Energy Reviews, 213, 115475.

Mouneer, S. (2025). CO2 emissions quandary of South Asia: Unraveling the influence of corruption and political stability: S. Mouneer. Environment, Development and Sustainability, 1-29.

Ng, J. H. C., Vyawahare, P., Benavides, P. T., Gan, Y., Sun, P., Boardman, R., . . . Elgowainy, A. (2025). Life-cycle greenhouse gas emissions associated with nuclear power generation in the United States. Journal of Industrial Ecology, 29(3), 719-732.

Paluszny, A., & Zimmerman, R. W. (2025). The role of subsurface geomechanics in the green energy transition. Royal Society Open Science, 12(5), 241516.

Reichardt, A., Murawski, M., & Bick, M. (2025). The use of the Internet of Things to increase energy efficiency in manufacturing industries. International Journal of Energy Sector Management, 19(2), 369-388.

Sahoo, R., Samanta, D., Sow, S., Ranjan, S., Nath, D., Sadhu, S., . . . Roy, D. K. (2025). Nexus between photosynthesis and radiation use efficiency towards achieving sustainability in the era of climate change: an overview. Discover Environment, 3(1), 67.

Scandurra, C., Mezza, F., Maldonato, N. M., Bottone, M., Bochicchio, V., Valerio, P., & Vitelli, R. (2019). Health of non-binary and genderqueer people: A systematic review. Frontiers in psychology, 10, 1453.

Schramm, L. (2025). Between Different National Preferences and Conflicting Policy Objectives: The Difficulties in Establishing a Common European Energy Policy. Contemporary European Politics, 3(1), e70001.

Tasev, G., Makreski, P., Jovanovski, G., Životić, D., Boev, I., & Jelenkovic, R. (2025). The environmental and health damage caused by the use of coal. ChemTexts, 11(1), 3.

Tissaoui, K., & Zaghdoudi, T. (2025). Against a background of energy uncertainty and climate change, is there a substitution effect between fossil fuels in OECD countries? Energy, 320, 135271.

Usman, M., Li, Q., Luo, D., Xing, Y., & Dong, D. (2025). Valorization of soybean by-products for sustainable waste processing with health benefits. Journal of the Science of Food and Agriculture, 105(10), 5150-5162.

Wang, C., Li, Y., Liao, Y., Tian, H., Huang, M., Dong, X., Du, J. (2018). 2018 Chinese Pediatric Cardiology Society (CPCS) guideline for diagnosis and treatment of syncope in children and adolescents. Science Bulletin, 63(23), 1558-1564.